ISSN: 2754-4753

Journal of Physics & Optics Sciences

SCIENTIFIC Research and Community

Research Article

Open Access

Matter Waves in the Talbot-Lau Interferometry

Valeriy I. Sbitnev[1,2]

[1]St. Petersburg B. P. Konstantinov Nuclear Physics Institute, NRC Kurchatov Institute, Gatchina, Leningrad district, 188300, Russia

[2]Department of Electrical Engineering and Computer Sciences, University of California, Berkeley, Berkeley, CA 94720, USA

ABSTRACT

Particle paths, emitted from distributed sources and passing out through slits of two gratings, G0 and G1, up to detectors, have been computed in detail by the path integral method. The particles under consideration are fullerene molecules with a De Broglie wavelength equal to 5 pm. The slits are Gaussian functions that simulate fuzzy edges of the slits. Waves of the matter computed by this method show perfect interference patterns both between the gratings and behind the second grating. Coherent and non-coherent distributed particle sources reproducing the interference patterns are discussed in detail. Paraxial approximation results from removing the distributed sources onto innity. This approximation gives a wave function reproducing an exact copy of the Talbot carpet. PACS numbers: 03.75.-b, 03.75.Dg, 42.25.Hz

***Corresponding author**

Valeriy I. Sbitnev, St. Petersburg B. P. Konstantinov Nuclear Physics Institute, NRC Kurchatov Institute, Gatchina, Leningrad district, 188300, Russia. Department of Electrical Engineering and Computer Sciences, University of California, Berkeley, Berkeley, CA 94720, USA; E-Mail: valery.sbitnev@gmail.com

Received: May 18, 2021; **Accepted:** May 25, 2021; **Published:** July 16, 2021

Introduction

Interferometry with matter waves, where particles are presented by heavy molecules, such as fullerene molecules, attracts the last years a great interest of the scientic community; see the review of Cronin, Schmiedmayer, and Pritchard and rich set of references ibid [1]. Interferometric experiments help to disclose the very basic principles of quantum physics with systems of rather large size and complexity [2-8].

Heavy molecules, having masses about 100 amu and more, are particles showing under or- dinary circumstances almost classical behavior. Indeed, diameter of the fullerene molecule C_{60}, see Fig. 1, is about 0.7 nm but de Broglie wavelength is ~ 5 pm (velocity of the molecule is about 100 m/s) [6,9,10]. The wavelength is

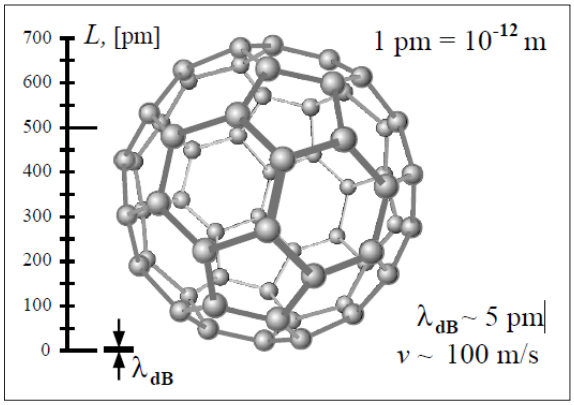

Figure 1: The fullerene molecule C60 consists of 60 carbon atoms. From the left, a characteristic size of the molecule together with its characteristic de Broglie wavelength are shown.

shorter than the diameter by a factor of 100 and much smaller than distances between atoms in a solid body, whereas the size of the molecule exceeds these distances. Interference fringes emer gent at scattering such heavy particles on a grating bear an important information about the wave-particle duality of these particles. Therefore, to reveal wave-particle duality for the heavy particles, interferometers should possess heightened requirements [7].

By adopting the wave-particle duality formalism relative to the heavy particles, one may then deal with ows of such particles as waves incident on the slit grating [11-14]. Methods based on computing the Fourier images of general two-dimensional periodic objects in light and electron optics can be proposed as good algorithms for nding interference patterns induced by the matter waves [15-18]. Next, a method adopted for the analytical description of diraction uses the Kirchho-Fresnel integral [6]. The integral represents spherical waves emitted from a radiation source. Because the integral is taken only over the slit, the slit appears to act as an effective source of radiation, following the Huygens principle [19]. This principle states that wavefronts passing through slits act as eective sources, reradiating spherical waves.

It is not intuitively obvious that the particles passing through the slits should be deected to recreate spherical wave patterns. The problem is that how does the particle identify positions of all slits? Nairz, Arndt, and Zeilinger have written "The wave-particle duality states that the description of the same physical object sug gests the local particle picture in the source and on the screen, but a wave model for the unob served propagation of the object [8]." While the particles go through the slits one by one, a single

Citation: Valeriy I. Sbitnev (2021) Matter Waves in the Talbot-Lau Interferometry. Journal of Physics & Optics Sciences. SRC/JPSOS/163.
DOI: doi.org/10.47363/JPSOS/2021(3)150

particle always gives a single click at a detector.

Between the source and the detector history of the particle remains unknown. We may consider all paths of point-like particles going through the slits and converging into the detector. This task is solved by the path integral method [20, 21]. The converging paths at the detector give rise to the superposition of dierent histories, which produce an interference phenomenon.

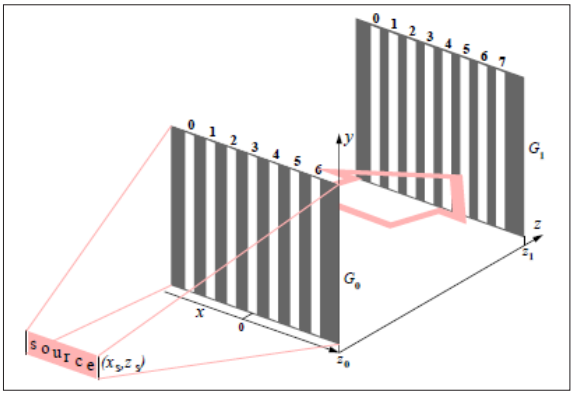

Figure 2: The Talbot-Lau interferometer scheme: two gratings, G0 and G1 are situated in consecutive order along a particle beam emitted from a distributed source.

Here we will consider the emergence of the interference patterns at passing fullerene-like particles through two gratings, G_0 and G_1, placed in consecutive order along a particle beam, see Fig. 2. It is a typical scheme of the TalbotLau interferometer [22, 23]. For nding the interference pattern we will compute all paths going from the source to the detector screen, i.e., we will compute the path integrals [?]. The emergence of the interference patterns is considered in the near-eld { the distance between the grating is half of the Talbot length, zT=2 = $d^2/\lambda_{dB} = z1 - z0$. Here dB is de Broglie wavelength and d is a distance between the slits.

Coherence properties of the beam are indispensable conditions for the manifestation of the wave-particle duality and, as an eect, the emergence of interference fringes. These properties depend on the source, collimation slits, and other extra conditions [8]. One distinguishes spatial coherence and spectral coherence. The rst is conditioned by the nite width of the source that can exceed the de Broglie wavelength. And the second can deteriorate because of generating the particles with dierent escaping velocities. Here we will try to reproduce both coherence properties. We will consider partially coherent sources, referred to as the generalized Gaussian Schell-model (GSM) sources [24-27]. Such sources reproduce planar GSM beams. These beams are characterized by two signs that are an intensity distribution across the beams and a spectral degree of coherence. Both are represented by the Gaussian distributions with their dispersion constants I and g. With suitable choices of I and g, such a source will simulate a beam, called GSM beam [24, 25].

Observe that the particle beam, according to the particle-wave duality, represents a matter- wave spreading through the grating device. It should be noted, that the wave consists of two parts, amplitude and phase ones multiplied each other, $|\Psi\rangle = \sqrt{\rho}\exp\{iS/\hbar\}$. $\rho = \langle\Psi|\Psi\rangle$. Only on the detector we register the intensity proportional to We will apply the Gaussian Schell model to the wave function as a simple Gaussian form-factor loaded by either of two dispersion constants σ_I and σ_g.

The article is organized as follows. In Sec. II we compute passing the particles through the two gratings, G_0 and G_1, being emitted from distributed sources. Exact formulas describing interference eect emergent both between the gratings and behind the second grating are represented in this section. Sec. III represents calculations of interference patterns emergent at scattering fullerene-like particles on the gratings with a nite amount of slits. Here we consider the eect of spatial coherence on interference patterns. In Sec .IV we remove the sources to innity and obtain the formulas for interference in the paraxial approximation. Here we consider an eect of spectral coherence. Sec. V discusses interference from the gratings with more hardedged slits. Sec. VI is concluding.

Path Integral: Particles Passing Through Slits in Two Screens

Computation of passing a particle through the system of two gratings, Fig. 2, is based on the path integral technique [21, 28]. Let both gratings be situated perpendicularly to axis z, see Fig. 3. We begin with writing the path integral that describes passing a particle both between the gratings and behind the second one. We believe, that between the screens the particle moves as a free particle. Its Lagrangian is

$$L = m\frac{\dot{x}^2}{2} + \text{const.} \qquad (1)$$

Here m is mass of the particle and x is its transversal velocity. A longitudinal momentum pz is much greater than its transverse component and we believe it is constant [8, 11, 13].

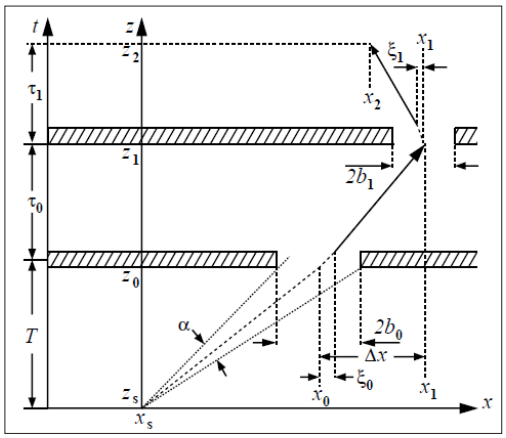

Figure 3: Passage of a particle along path xs → x_0 → x_1 → x_2 through two screens containing slits with widths $2b_0$ and $2b_1$.

The particles flying through the rst slit along a ray will pass this slit, located from $x_0 - b_0$ to $x_0 + b_0$, almost surely. And let its deviation after passing the rst slit be such, that it passes through the second slit located from $x_1 - b_1$ to $x_1 + b_1$. The path integral in that case reads

$$\begin{aligned}
&\psi(x_2, x_1, x_0, x_s) \\
&= \int_{-b_1}^{b_1} K(x_2, T+\tau_0+\tau_1; x_1+\xi_1, T+\tau_0) \\
&\quad \int_{-b_0}^{b_0} K(x_1+\xi_1, T+\tau_0; x_0+\xi_0, T) \\
&\quad \times K(x_0+\xi_0, T; x_s, 0) d\xi_0 d\xi_1. \qquad (2)
\end{aligned}$$

Integral kernels (propagators) for the particle freely flying are as follows [21].

$$K(x_b,t_b;x_a,t_a) = \left[\frac{2\pi\mathbf{i}\hbar(t_b-t_a)}{m}\right]^{-1/2}\exp\left\{\frac{\mathbf{i}m(x_b-x_a)^2}{2\hbar(t_b-t_a)}\right\}. \tag{3}$$

By substituting the propagators into the path integral (2) we get

$$\psi(x_2,x_1,x_0,x_s) = \int_{-b_1}^{b_1}\left(\frac{2\pi\mathbf{i}\hbar\tau_1}{m}\right)^{-1/2}\exp\left\{\frac{\mathbf{i}m(x_2-(x_1+\xi_1))^2}{2\hbar\tau_1}\right\}$$
$$\int_{-b_0}^{b_0}\left(\frac{2\pi\mathbf{i}\hbar\tau_0}{m}\right)^{-1/2}\exp\left\{\frac{\mathbf{i}m((x_1+\xi_1)-(x_0+\xi_0))^2}{2\hbar\tau_0}\right\}\left(\frac{2\pi\mathbf{i}\hbar T}{m}\right)^{-1/2}\exp\left\{\frac{\mathbf{i}m((x_0+\xi_0)-x_s)^2}{2\hbar T}\right\}d\xi_0 d\xi_1.$$

The both integrals we can see are computed within nite intervals [–*b*0;+*b*0] and [–*b*1;+*b*1], respectively. Observe, that the integrating can be broadened from –∞ to +∞. But in this case, we need to load the integrals by the step functions equal to the unit within the nite intervals [–*b*0;+*b*0] and [–*b*1;+*b*1] and they vanish outside of the intervals.

To obtain exact solutions of the path integral let us take the supposition, that the slits possess slightly fuzzy edges. In that case, the form factors, simulating the slits, can be represented by the Gaussian function [21]

$$G(\xi) = \exp\{-\xi^2/2b^2\}. \tag{5}$$

The eective width of the Gaussian curve is given by the parameter *b*. About two-thirds of the area of the curve is placed between points –*b* and +*b*, and one-third of the area is beyond the interval (–*b*;+*b*). It means, in the vicinity of the slits tunneling through the semi-transparent screen can take place. It is due to the fuzzy edges adopted above.

Let us insert into the integrals the Gaussian factors $G(\xi_0)$ and $G(\xi_1)$ with the parameters b_0 and b_1 and replace the nite limits b_0 and b_1 by the limits from –∞ to +∞. Since we have a solution for the inner integral, that has been written out in we can rewrite the integral (4) more denitely [29].

$$\psi(x_2,x_1,x_0,x_s) = \left(\frac{1}{T}+\frac{1}{\tau_0}+\frac{\mathbf{i}\hbar}{mb_0^2}\right)^{-1/2}\int_{-\infty}^{\infty}\frac{mG(\xi_1)}{2\pi\mathbf{i}\hbar\sqrt{T\tau_0\tau_1}}\exp\left\{\frac{\mathbf{i}m(x_2-(x_1+\xi_1))^2}{2\hbar\tau_1}\right\}$$
$$\times\exp\left\{\frac{\mathbf{i}m}{2\hbar}\left(\left(\frac{((x_1+\xi_1)-x_0)^2}{\tau_0}+\frac{(x_0-x_s)^2}{T}\right)-\frac{(-((x_1+\xi_1)-x_0)/\tau_0+(x_0-x_s)/T)^2}{(1/\tau_0+1/T+\mathbf{i}\hbar/mb_0^2)}\right)\right\}d\xi_1. \tag{6}$$

Solutions of such integrals stem from the formula $\int_{-\infty}^{\infty}\mathrm{e}^{\alpha\xi^2+\beta\xi+\gamma}\,d\xi = \sqrt{\frac{\pi}{-\alpha}}\,\mathrm{e}^{-\beta^2/4\alpha+\gamma}$. (7)

To get such a form, let us regroup all terms under the integral (6) and collect them at coecients ξ_1^2, ξ_1 and free from it. We find

1. the term at ξ_1^2

$$\alpha = \frac{\mathbf{i}m}{2\hbar}\left(\frac{1}{\tau_1}+\frac{1}{\tau_0}+\frac{\mathbf{i}\hbar}{mb_1^2}-\frac{1}{\tau_0^2(1/\tau_0+1/T+\mathbf{i}\hbar/mb_0^2)}\right); \tag{8}$$

2. the term at ξ_1

$$\beta = -2\frac{\mathbf{i}m}{2\hbar}\left(\frac{(x_2-x_1)}{\tau_1}-\frac{(x_1-x_0)}{\tau_0}+\frac{(x_1-x_0)/\tau_0^2-(x_0-x_s)/\tau_0 T}{(1/\tau_0+1/T+\mathbf{i}\hbar/mb_0^2)}\right); \tag{9}$$

3. the term free from ξ_1

$$\gamma = \frac{\mathbf{i}m}{2\hbar}\left(\frac{(x_2-x_1)^2}{\tau_1}+\frac{(x_1-x_0)^2}{\tau_0}+\frac{(x_0-x_s)^2}{T}-\frac{((x_1-x_0)/\tau_0-(x_0-x_s)/T)^2}{(1/\tau_0+1/T+\mathbf{i}\hbar/mb_0^2)}\right).$$

Now we can express the terms (=(π / (–α))$^{1/2}$ and γ–β^2/4α given in the right part of Eq. (7). The first term, accurate to the multiplicand

$$\left(\frac{1}{T}+\frac{1}{\tau_0}+\frac{\mathbf{i}\hbar}{mb_0^2}\right)^{-1/2}\frac{m}{2\pi\mathbf{i}\hbar\sqrt{T\tau_0\tau_1}}, \tag{11}$$

relates to an amplitude factor A of the wave function $\psi(x_2; x1; x0; xs)$ written in a general view in Eq. (4). For this reason, by multiplying the term (π/ (–α))$^{1/2}$ by the multiplicand (11) we obtain this factor:

$$A=\sqrt{\frac{m}{2\pi\mathbf{i}\hbar T}}\cdot\frac{1}{\sqrt{\left(1+\frac{\tau_1}{\tau_0}\right)\left(1+\frac{\mathbf{i}\hbar\tau_1}{mb_1^2(1+\tau_1/\tau_0)}\right)\left(1+\frac{\tau_0}{T}\right)\left(1+\frac{\mathbf{i}\hbar\tau_0}{mb_0^2(1+\tau_0/T)}\right)-\frac{\tau_1}{\tau_0}}}. \tag{12}$$

In turn, the term $\gamma-\beta^2/4\alpha$ reads:

$$\gamma-\beta^2/4\alpha=\frac{\mathbf{i}m}{2\hbar}\left[\left(\frac{(x_2-x_1)^2}{\tau_1}+\frac{(x_1-x_0)^2}{\tau_0}+\frac{(x_0-x_s)^2}{T}-\frac{((x_1-x_0)/\tau_0-(x_0-x_s)/T)^2}{((\tau_0+T)/T\tau_0+\mathbf{i}\hbar/mb_0^2)}\right)-\frac{\left(\frac{(x_2-x_1)}{\tau_1}-\frac{(x_1-x_0)}{\tau_0}+\frac{(x_1-x_0)/\tau_0-(x_0-x_s)/T}{\tau_0((\tau_0+T)/T\tau_0+\mathbf{i}\hbar/mb_0^2)}\right)^2}{\left(\frac{\tau_0+T}{T\tau_0}+\frac{\mathbf{i}\hbar}{mb_0^2}\right)^{-1}\left(\left(\frac{\tau_1+\tau_0}{\tau_1\tau_0}+\frac{\mathbf{i}\hbar}{mb_1^2}\right)\left(\frac{\tau_0+T}{T\tau_0}+\frac{\mathbf{i}\hbar}{mb_0^2}\right)-\frac{1}{\tau_0^2}\right)}\right] \tag{13}$$

Series of Replacements

To make th expression (13) less cumbersome, let us dene and name some terms as generalized terms. First, we dene eective slit's half-widths

$$\sigma_{j,0}=\frac{b_j}{\sqrt{2}}, \tag{14}$$

where *j* takes numbers 0 and 1. And next, we determine a time-dependent complex-valued spreading

$$\sigma_{j,\tau_j} = \sigma_{j,0}+\mathbf{i}\frac{\hbar\tau_j}{2m\sigma_{j,0}(1+\tau_j/\tau_{j-1})} \tag{15}$$

where $j = 0$; 1 and at $j = 0$ we suppose $\tau_{-1} = T$. It should be noted, the complex spreading parameters have been presented in works [30, 31]. Here we choose the same representation.

More one step is to replace ight times T, τ_0, and τ_1 by flight distances $(z_0 – z_s)$, $(z_1–z_0)$, and (z2 – z1), Fig. 3. This replacement reads

$$\begin{cases} T=(z_0-z_s)/v_z, \\ \tau_0=(z_1-z_0)/v_z, \\ \tau_1=(z_2-z_1)/v_z, \end{cases} \tag{16}$$

where vz is a particle velocity along the axis z. We note that mvz = pz is z-component of the particle momentum. Next, we introduce the de Broglie wavelength $\lambda_{dB} = h/pz$, where $h = 2\pi\hbar$ is the Planck constant, and rewrite the expression (15) according to these remarks

$$\sigma_{j,\tau_j\to z_j} = \sigma_{j,0}+\mathbf{i}\frac{\lambda_{dB}(z_{j+1}-z_j)}{4\pi\sigma_{j,0}\left(\frac{z_{j+1}-z_{j-1}}{z_j-z_{j-1}}\right)}. \tag{17}$$

Hereinafter, for brevity, we will not write the subscript dB at λ meaning de Broglie's wave-length.

Let us dene a dimensionless distance dependent complex-valued spreading as follows

$$\begin{aligned}\Sigma_{j,z_j} &= \left(\frac{z_{j+1}-z_{j-1}}{z_j-z_{j-1}}\right)\frac{\sigma_{j,z_j}}{\sigma_{j,0}} \\ &= \frac{z_{j+1}-z_{j-1}}{z_j-z_{j-1}}+\mathbf{i}\frac{\lambda(z_{j+1}-z_j)}{4\pi\sigma_{j,0}^2}.\end{aligned} \tag{18}$$

Also we dene a dimensionless parameter

$$\Xi_0=1-\frac{(x_0-x_s)}{(z_0-z_s)}\frac{(z_1-z_0)}{(x_1-x_0)} \tag{19}$$

that tends to 1 as $z_s \to -\infty$ – the source is removed to innity. Now we can rewrite the terms A and $\gamma-\beta^2/4\alpha$, represented in Eqs. (12) and (13), by replacing cumbersome parameters by dened above.

The amplitude factor, A, of the wave function $\psi(x_2, x_1, x_0, xs)$ has the following view

$$A=\sqrt{\frac{m}{2\pi\mathbf{i}\hbar T}}\cdot\frac{1}{D(\Sigma_{0,z_0},\Sigma_{1,z_1})}. \tag{20}$$

Here we do not replace T by $(z_0 - z_s) / vz$. It points out to distance to the source accurate to division by vz. As we remove the sources to innity ($T \to \infty$) the amplitude factor tends to zero. Nevertheless, we keep a nite value of the parameter A as a normalization factor of the wave function [29].

The phase term, $\gamma - \beta^2 / 4\alpha$ for the same wave function $\psi(x_2, x_1, x_0, x_s)$ reads

$$\gamma - \beta^2/4\alpha = i\pi \left[\left(\frac{(x_2 - x_1)^2}{\lambda(z_2 - z_1)} + \frac{(x_1 - x_0)^2}{\lambda(z_1 - z_0)} \left(1 - \frac{\Xi_0^2}{\Sigma_{0,z_0}} \right) + \frac{(x_0 - x_s)^2}{\lambda(z_0 - z_s)} \right) - \frac{\lambda(z_2 - z_1)\Sigma_{0,z_0}}{D(\Sigma_{0,z_0}, \Sigma_{1,z_1})^2} \left(\frac{(x_2 - x_1)}{\lambda(z_2 - z_1)} - \frac{(x_1 - x_0)}{\lambda(z_1 - z_0)} \left(1 - \frac{\Xi_0}{\Sigma_{0,z_0}} \right) \right)^2 \right], \tag{21}$$

The term D $(\sum_0, z_0, \sum_1, z_1)$ represented in divisors of expressions (20) and (21) is as follows

$$D(\Sigma_{0,z_0}, \Sigma_{1,z_1}) = \sqrt{\Sigma_{0,z_0}\Sigma_{1,z_1} - \frac{z_2 - z_1}{z_1 - z_0}}. \tag{22}$$

Matter waves behind the gratings G_0 and G_1

For observation of the wave eld behind the second grating, G_1, we situate a detector in a point $(x_2; z_2)$, Fig. 3. On the other hand, if we wish to observe the wave-eld between the first and second gratings, between G_0 and G_1, we must situate the detector in a point $(x_1; z_1)$. In order to realize the second case, it is sucient to put in the expressions (21) and (22) $x_2 = x_1$ and $z_2 = z_1$. Let now the point $(x_2; z_2) = (x_1; z_1)$ be situated in a region between the gratings. Observe, in this case, that all terms containing differences $(z_2 - z_1)$ vanish. Next, we move the detector in the point $(x_1, z_1) \to (x, z)$ that can be situated anywhere between the gratings.

We note that the expressions (21) and (22) contain full information about wave-elds both between the gratings and behind the second grating. It depends on choosing coordinates of position of the detector, either $z_2 \to z$, $x_2 \to x$, or $z_2 = z_1 \to z$, $x_2 = x_1 \to x$. We write variables (x, z) instead of (x_2, z_2) at describing the wave-eld behind the second grating. Let us also write the same variables (x, z) instead of $(x_1; z_1)$ when we describe the wave pattern between the gratings. In the last case, we have replacements $(z_2 - z_1) \to (z - z_1) \to (z - z) = 0$, $(x_2 - x_1) \to (x - x_1) \to (x - x) = 0$, Terms containing such dierences either vanish or become unit if a ratio $(x - x) / (z - z)$ takes place. Now we can write out the wave patterns at passing the particle through a single slit within each grating.

A particle emitted from the point (xs, Zs) belonging to the source, can be detected in the point (x, z), $z > z_1$ (we mean behind the second grating, $(x_2, z_2) \equiv (x, z)$) in accordance with the following wave function

$$\psi(x, z, x_1, x_0, x_s) = \frac{\sqrt{\frac{m}{2\pi i\hbar T}}}{D(\Sigma_{0,z_0}, \Sigma_{1,z_1})} \exp\left\{ i\pi \left[\left(\frac{(x - x_1)^2}{\lambda(z - z_1)} + \frac{(x_1 - x_0)^2}{\lambda(z_1 - z_0)} \left(1 - \frac{\Xi_0^2}{\Sigma_{0,z_0}} \right) + \frac{(x_0 - x_s)^2}{\lambda(z_0 - z_s)} \right) - \frac{\lambda(z - z_1)\Sigma_{0,z_0}}{D(\Sigma_{0,z_0}, \Sigma_{1,z_1})^2} \left(\frac{(x - x_1)}{\lambda(z - z_1)} - \frac{(x_1 - x_0)}{\lambda(z_1 - z_0)} \left(1 - \frac{\Xi_0}{\Sigma_{0,z_0}} \right) \right)^2 \right] \right\}$$

In the region between the gratings, $z < z_1$, we employ replacement $(x_1, z_1) \Rightarrow (x, z)$ and consequently

$$\psi(x, z, x_0, x_s) = \sqrt{\frac{m}{2\pi i\hbar T \Sigma_{0,z_0}}} \cdot \exp\left\{ i\pi \left[\frac{(x - x_0)^2}{\lambda(z - z_0)} \left(1 - \frac{\Xi_0^2}{\Sigma_{0,z_0}} \right) + \frac{(x_0 - x_s)^2}{\lambda(z_0 - z_s)} \right] \right\} \tag{24}$$

As we stated above, the function $\psi(x, z, x_0, xs)$ stems from $\psi(x, z, x_1, x_0, xs)$ as soon as we put in Eq. (23) values $z_1 = z$ and $x_1 = x$. Observe, that $D(\sum_{0,z_0}, \sum_1 z_1) = \sum_1^{1/2}{}_{z_0}$, so far as $\sum_1, z_1 = 1$ at $z = z_1 = z_2$, see Eqs. (18) and (22).

Interference Patterns from Two-Grating Structure

The gratings shown in Fig. 2 we believe have dierent amount of slits. The rst grating has N_0 slits, so $n_0 = 0, 1....(N_0 - 1)$. The second grating has N_1 slits, and $n_1 = 0, 1....,(N_1 - 1)$.

Distance between slits for the rst grating is d_0 and for the second grating is d_1. Now we can write out a wave-eld beyond the gratings that is composed of a superposition of wave functions representing coherent emission from all slits.

The matter-wave in a zone between the first and second gratings reads

$$|\Psi_0(x,z,x_s,\lambda)\rangle = \sum_{n_0=0}^{N_0-1}\psi\left(x,z,\left(n_0-\frac{N_0-1}{2}\right)d_0,x_s\right). \quad (25)$$

And the matter-wave extending beyond the second grating reads

$$|\Psi_1(x,z,x_s,\lambda)\rangle = \sum_{n_1=0}^{N_1-1}\sum_{n_0=0}^{N_0-1}\psi\left(x,z,\left(n_1-\frac{N_1-1}{2}\right)d_1,\left(n_0-\frac{N_0-1}{2}\right)d_0,x_s\right). \quad (26)$$

Both wave functions are represented without normalized factors. We need no here in these factors since our interest is to show a general pattern of the density distribution

$$p(x,z) = \langle\Psi(x,z,x_s,\lambda)|\Psi(x,z,x_s,\lambda)\rangle. \quad (27)$$

As for the particles supporting the matter- wave here, we consider fullerene molecules [10]. They are massive molecules. Its mass is about $mC60 \approx 1.2 \times 10^{-24}$ kg. The fullerene molecule has radius $RC_{60} = 350$ pm [9]. In turn, the de Broglie wavelength is much smaller than this radius. For instance, the de Broglie wavelength equal to 5 pm appears in the experimental work [10]. The wavelength $\lambda dB = 5$ pm is adopted in this work as well. The widths of the slits (open slit windows) are as small as $2b0 = 75$ nm in $G0$ and $2b1 = 150$ nm in $G1$. Distances between the slits are equivalent for both gratings $d0 = d1 = 500$ nm. The distances have been double increased in contrast to those given in [10] and [29]. It is done so that we could see denitely the Talbot carpets arising between the gratings, and maybe beyond the both gratings.

Here we consider example of emergence of in- terference patterns from the gratings G_0 and G_1 containing even amount of slits, $N_0 = 32$, and odd amount of slits, $N1 = 33$. The dierence in parity of the numbers N0 and N1 is conditioned by the fact, that the rst self-image of the grating $G0$ is shifted exactly on the half period of the grating. Due to this trick, the slits of the grating $G1$ are located exactly on nodes of the rst self-image of the grating $G0$. It means that the grating $G1$ keeps "open gates" for particles to spread further.

Fig. 4 shows the density distribution $p(x, z)$ in the near-eld region. Hereandfurther we will use a natural interference length named the Talbot length $zT = d^2/\lambda dB$.

The point source of radiation is placed on 0.5 m apart from the rst grating, $zs = –0:5$ m. And it has dierent locations along the axis x: (a) $x_s = 0$ μm; (b) $x_s = 2$ μm; and (c) $x_s = 4$ μm. Here we have shown cases of shifting the point source to a positive area, $x_s > 0$. As for negative shifting, it can be obtained by simple reflection of the interference patterns about the plane (y,z) intersecting axis x at $x = 0$. That is, numerations of the slits should be subjected to the following inversion 12↔19, 13↔18, 14↔17, 15↔16.

In Figs. 4(a), 4(b), and 4(c) one can see ripples of high order against the background of the basic divergent rays. They are induced by the presence of many lateral slits invisible in these gures. The interference patterns are seen to vary as the position of the point source changes.

Coherent and Non-coherent Sources

Let us now turn to the coherence properties of the particle beam [8]. One assumes, that point

Citation: Valeriy I. Sbitnev (2021) Matter Waves in the Talbot-Lau Interferometry. Journal of Physics & Optics Sciences. SRC/JPSOS/163.
DOI: doi.org/10.47363/JPSOS/2021(3)150

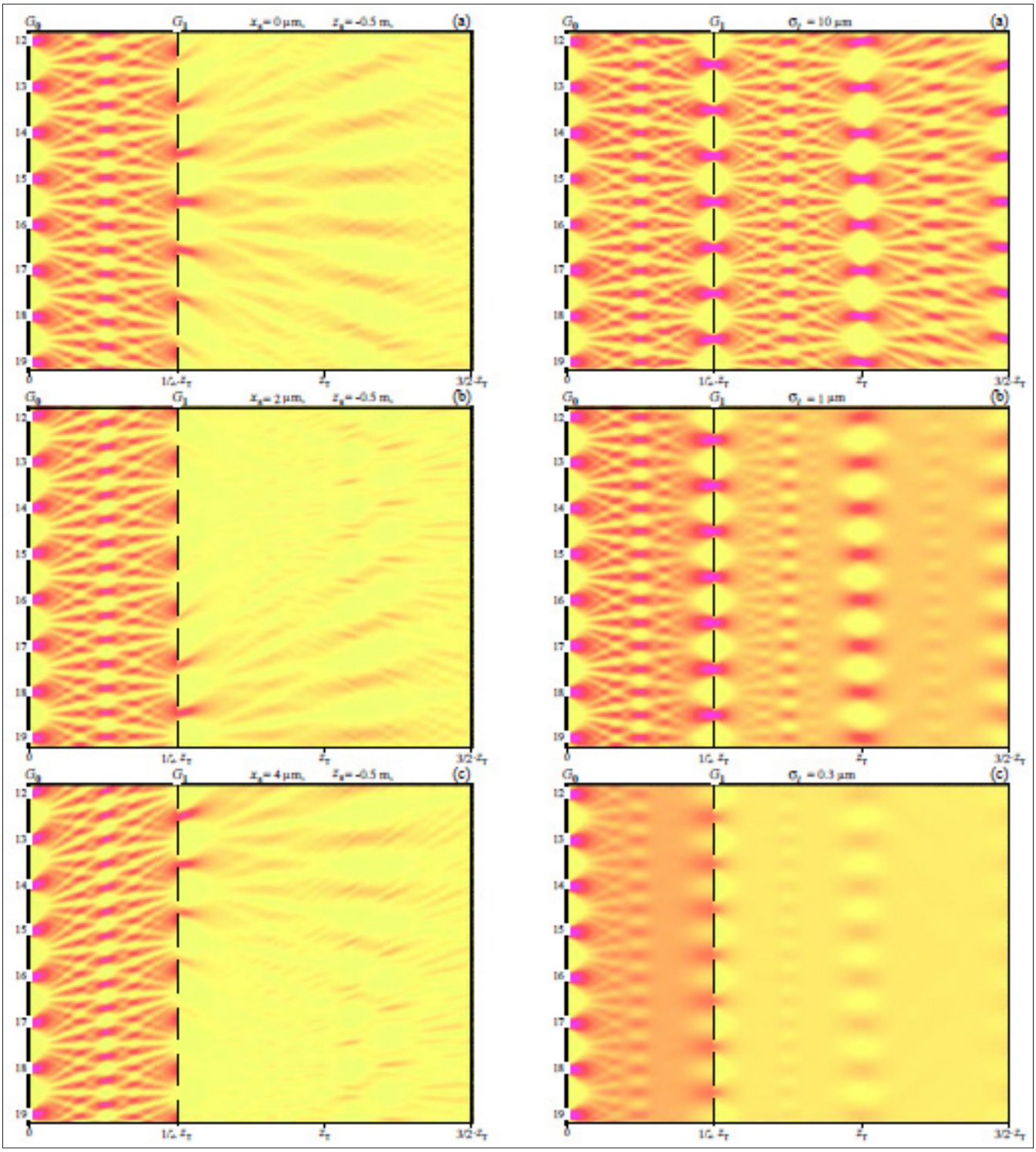

Figure 4: Density distribution pattern p(x; z) in the neareld region z 2 (0, 1:5z_T) = (0, 0.15) m, N_0 = 32, N_1 = 33, de Broglie wavelength dB = 5 pm, Talbot length z_T = 0.1 m. Distance from G_0 to the source is z_S = –0:5 m : (a) the source is situated on the optical axis, xs = 0; (b) the source is shifted from the central axis on xs = 2 μm; (c) the source is shifted from the central axis on xs = 4 μm .

Figure 4: Density distribution pattern p(x, z) averaged over all point sources localized with increment δxs = 0:25 μm in the interval $xs \in$ [–4, 4] μm, zs = –0:5 m, N_0 = 32, N_1 = 33. The averaging has been carried out with the Gaussian kernel (29) loaded by the dispersion constant I : (a) coherent beam, σ_I = 10 μm; (b) almost coherent beam, σ_I = 1 μm; (c) almost noncoherent beam, σ_I = 0:3 μm.

sources are coherent, if wave functions relating to these sources are summed up in the vicinity of a detector. And they are non-coherent if instead of the wave functions their intensities (probability densities) are summed up. We have to keep in mind that the wave functions are primary quantum subjects, whereas intensities are found on a nal stage at reading from detectors. The wave functions bear more full information about a quantum object, than their intensities where the information loses partially because of the averaging. In particular, super position of the wave functions in the vicinity of the detector can give a weakened contribution of cross-terms, which provide interference eects. This case relates to intermediate variants, which can be considered by appealing to the Gaussian Schell-model [24, 25].

Averaging of the wave functions from all point sources distributed along *xs* at fixed *zs* is carried out as follows:

$$p(x,z) = \sigma_I \sum_{x_s'} \sum_{x_s''} \langle \Psi(x,z,x_s',\lambda) | \mu(x_s',x_s'',\sigma_I) | \Psi(x,z,x_s'',\lambda) \rangle. \quad (28)$$

The Gaussian kernel $\mu(x_s', x_s'', \sigma_I)$ reads

$$\mu(x_s', x_s'', \sigma_I) = \frac{1}{\sqrt{2\pi}\,\sigma_I} \exp\left\{ -\frac{(x_s' - x_s'')^2}{2\,\sigma_I^2} \right\} \quad (29)$$

with the dispersion parameter σ_I being an eective coherent width of the beam. This parameter presented as a factor in front of the sums (28) provides the identity of dimensionalities for the probability density distributions.

First, one can notice that at $\sigma_I << 1$, the Gaussian kernel ts the Dirac -function. And the expression (28) drops to a simple summation of the probability densities

$$p(x,z) \sim \sum_{x_s} \langle \Psi(x,z,x_s,\lambda) | \Psi(x,z,x_s,\lambda) \rangle. \quad (30)$$

And at $\sigma_I >> 1$ the Gaussian kernel degenerates to a constant. In that case, we have

$$p(x,z) \sim \sum_{x_s} \langle \Psi(x,z,x_s,\lambda) | \Psi(x,z,x_s,\lambda) \rangle + \sum_{x_s' \neq x_s''} \sum_{x_s''} \langle \Psi(x,z,x_s',\lambda) | \Psi(x,z,x_s'',\lambda) \rangle. \quad (31)$$

The second sum here contains the cross terms, that introduce interference eects from dierent point sources.

The expression (30) represents an example of a wholly noncoherent beam. Whereas, the expression (31) gives a completely coherent beam. Intermediate coherence beams are possible as well.

Figs. 5(a), 5(b), and 5(c) show averaged density distributions for dierent depth of coherence of incident beam.

Summation is taken for all point sources localized at $xs = -4$, $-3.25, -3.5, \ldots, 4$ μm, the increment is $\delta xs = 0.25\,\mu$m. Distance to the source is $zs = -0.5$ m. The gures demonstrate interference patterns that are reproduced from (a) coherent beam, $\sigma_I = 10\,\mu$m, to (c) almost non coherent beam, $\sigma_I = 0.3\,\mu$m. The high-order interference fringes are seen to be washed out as the dispersion parameter σ_I decreases from 10 μm to 0.1 μm, which is in good agreement with computational results given in [32].

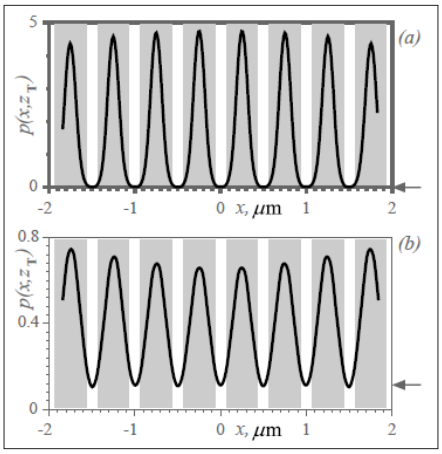

Figure 6: Interference fringes observed in the cross-section of the density distribution pattern (28) at $z = z_T$: (a) almost coherent beam, $\sigma_I = 1\,\mu$m; (b) noncoherent beam, $\sigma_I = 0.1\,\mu$m Gray vertical strips indicate opaque spaces between slits in the grating G_1. Arrow points out a level of pedestal.

Let us put a detector screen on the distance $L = z_T$ from the grating G_0. Look out on emergent interference fringes for two cases, namely, for $\sigma_I = 1\,\mu$m and for $\sigma_I = 0.1\,\mu$m, see Figs. 6(a) and 6(b). One can see, that at decreasing the dispersion parameter σI a pedestal supporting the interference fringes emerges. The position of the pedestal is pointed out by arrow in Fig. 6.

The pedestal can be found as an absolute minimum for all the interference fringes

$$P_{\min} = \min_{\forall x} p(x, z_T) \quad (32)$$

We can nd also an absolute maximum

$$P_{\max} = \max_{\forall x} p(x, z_T) \quad (33)$$

The interferometric visibility is computed by a formula [32]

$$V = \frac{P_{\max} - P_{\min}}{P_{\max} + P_{\min}} \quad (34)$$

quanties the contrast of the interference fringes.

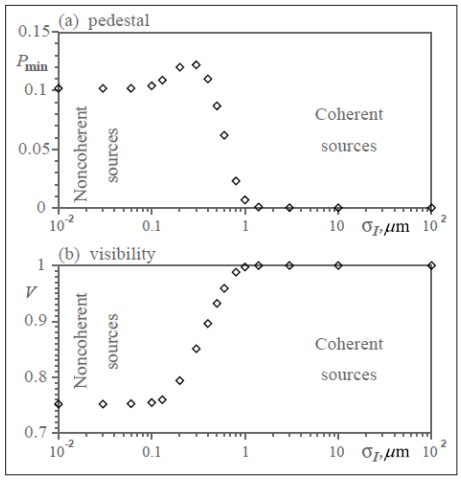

Figure 7: Pedestal P_{min} (a) and visibility V (b) calculated as functions of the eective coherent width σ_I of the beam.

Variations of two parameters, level of the pedestal P_{min} and the visibility V, simulated as functions of the eective coherent width of the beam σ_l ranging from $10^{-2}\,\mu$m to $10^{2}\,\mu$m are shown in Figs. 7(a) and 7(b). A crossover is clearly seen within the interval 1 μm down to 0.1 μm. It represents a smooth transition from the coherent source to noncoherent as the dispersion parameter σ_l decreases within the mentioned interval.

Surprisingly, if radiation from all point sources, all situated near the interferometer, is coherent, the superposition of these radiations reproduces a perfect interference pattern as if from a single remote source, see Fig. 5(a). At that, all point sources situated near the grating G_0 demonstrate radial divergence of rays beyond the grating G_1, as is seen in Figs. 4(a)-(c). To see a general pattern of such a radial divergence we have simulated the emergence of an interference pattern from two gratings consisting of $N_0 = 32$ and $N_1 = 33$ slits. Fig. 8(a) shows this interference pattern. Because of closely spaced the single source, $z_S = -0.5$ m, we see, that there are three groups of divergent rays from the second grating.

Lateral rays of these groups interfere on a distance of the half Talbot length from the second grating. It is remarkable, that the superposition of these divergent rays from dierent coherent sources reproduces the Talbot-like interference pattern as shown in Fig. 5(a).

Fig. 8(b) demonstrates the very interference but for the point source on $z_S = -50$ m distant from the grating $G0$. One can believe in this case, that the source has been removed almost to innity. One can see, that Fig. 8(b) displays in the near-eld the Talbot carpets, that continue behind the second grating. For the emergence of the perfect Talbot carpet, it is necessary to satisfy the following three requirements [33–35]: (a) a particle beam is paraxial; (b) ratio of de Broglie wavelength, λ_{dB}, to the period of a grating, d, tends to zero; (c) number of the slits tends to innity. Fig. 9 shows the Talbot carpet emergent from the two gratings conguration consisting of $N_0 = 64$ and $N_1 = 63$ slits. The Talbot carpet looks the better, the more number of the slits is in the gratings, ideally tending to inn ity [36].

It is instructive to compare patterns shown in Figs. 5(a) and 9. The rst Talbot-like pattern was got by superposing many coherent rays arising from sources situated near the interferometer. This pattern is washed out as soon as the rays become noncoherent. Whereas the second Talbot pattern is got from a single plane wave incident to the interferometer from innity. Observe that in the case of the coherent

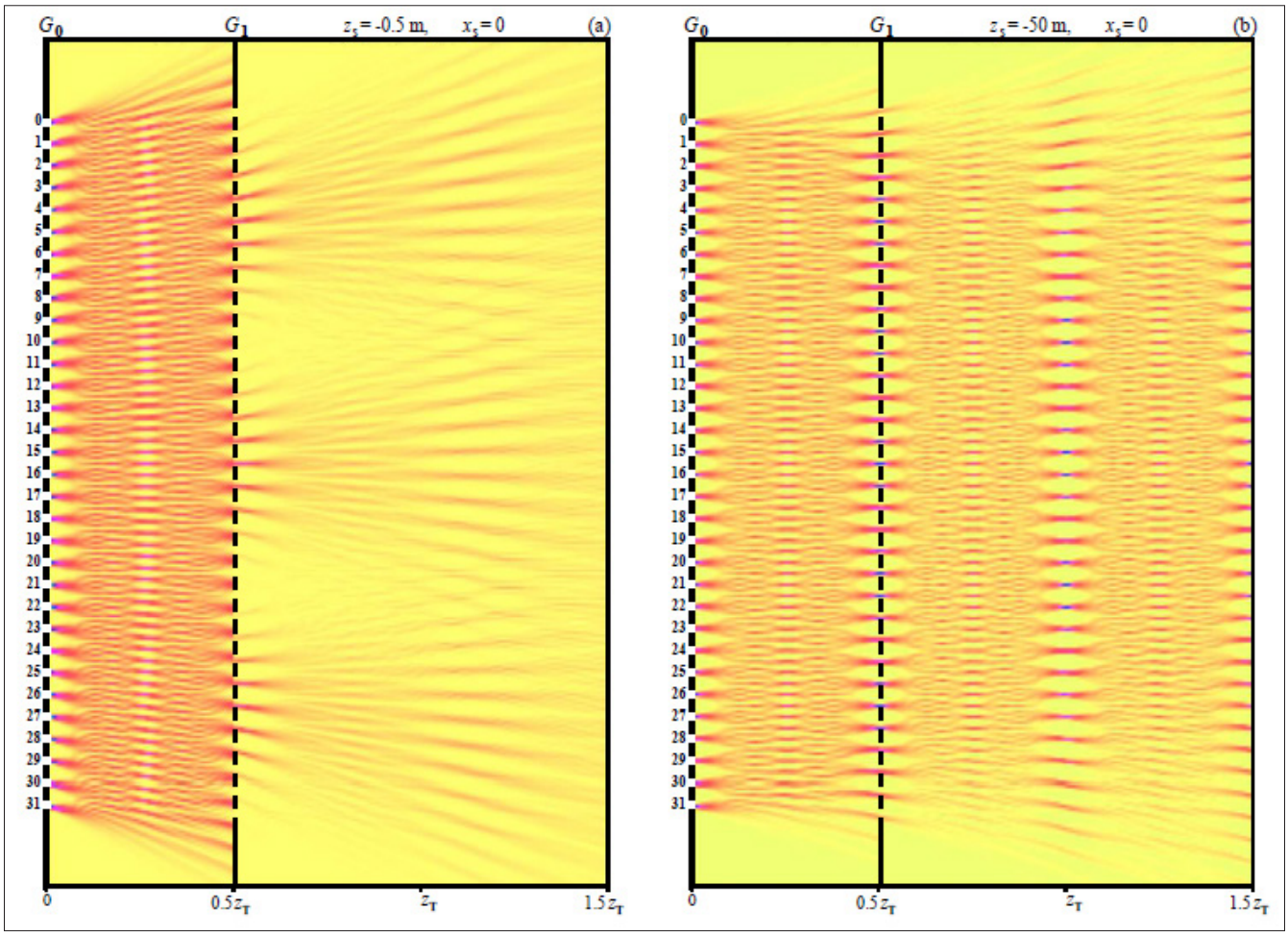

Figure 8: The density distribution pattern $p(x, z)$: (a) particle source is spaced closely to the rst grating, $z_S = -0.5$ m; (b) particle source is spaced far from the rst grating, $z_S = -50$ m. De Broglie wave length $\lambda_{dB} = 5$ pm, and $z_T = 0.1$ m.

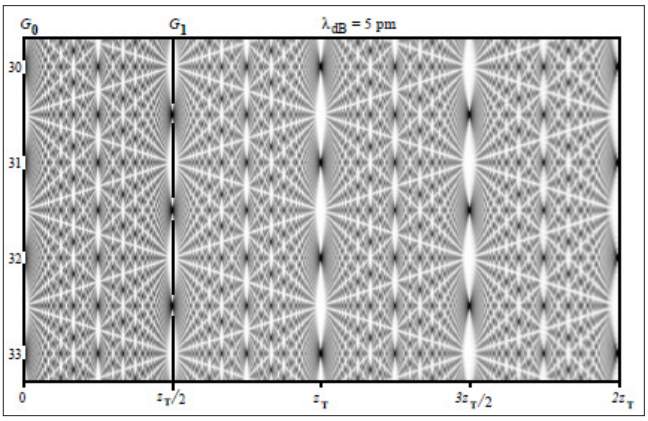

Figure 9: Talbot carpet on two grating conguration: the gratings G_0 and G_1 consists of $N0 = 64$ and $N1 = 63$ slits, respectively. De Broglie wavelength $\lambda_{dB} = 5$ pm, distance between slits $d = 500$ nm, the Talbot length $z_T = 0.1$ m.

monochromatic beam, the presence of the second grating does not aect emergent interference patterns. That is, the same interference pattern emerges if we would remove the second grating.

Briey, the incident beam shows spherical equal-phase surfaces of the matter-wave when the source is positioned nearby the interferometer. At removing the source onto innity, the spherical equal-phase surfaces degenerate into planar equal-phase surfaces. In that case, the spherical wave turns into the plane wave incident on the interferometer. The particles' momenta are perpendicular to the equal-phase surface and particles pass in parallel to the axis of the optical system, the axis z. Such a particle beam is called the paraxial beam. In the next section, we obtain this paraxial approximation.

Paraxial approximation

The wave functions (23)-(24) gives description of interference in the paraxial approximation when a limit zs $\to -\infty$ is reached. Observe, that in this limit $\Xi_0 = 1,\ \Sigma_{0,z_0} = \sigma_{0,z_0}/\sigma_{0,0}$ and taking into account (14) and (17) we find

$$\frac{\mathbf{i}\pi}{\lambda_{\rm dB}(z_1-z_0)}\left(1-\frac{1}{\Sigma_{0,z_0}}\right)=-\frac{1}{4\sigma_{0,0}\,\sigma_{0,z_0}}=-\frac{1}{2b^2\left(1+\mathbf{i}\dfrac{(z_1-z_0)\lambda_{\rm dB}}{2\pi b^2}\right)} \tag{35}$$

Next, we need also to reinterpret the term $D(\Sigma_{0,z_0},\Sigma_{1,z_1})\to D(\sigma_{0,z_0},\sigma_{1,z_1})$:

$$D(\sigma_{0,z_0},\sigma_{1,z_1})=\sqrt{\left(\frac{z-z_0}{z_1-z_0}\right)\frac{\sigma_{1,z_1}}{\sigma_{1,0}}\frac{\sigma_{0,z_0}}{\sigma_{0,0}}-\left(\frac{z-z_1}{z_1-z_0}\right)}. \tag{36}$$

It is instructive to compare this expression with Eq. (22) representing the term D ($\sum_0$, z_0, $\sum_1$, z_1).

As soon as all reductions have been done, we obtain the wave function in the paraxial approximation, i.e., the source remote onto innity. It has the following view

$$\begin{aligned}\psi(x,z,x_1,x_0) \;=\; &\frac{A_\infty}{D(\sigma_{0,z_0},\sigma_{1,z_1})}\exp\left\{\mathbf{i}\pi\left[\left(\frac{(x-x_1)^2}{\lambda(z-z_1)}+\mathbf{i}\,\frac{(x_1-x_0)^2}{4\pi\sigma_{0,0}\sigma_{0,z_0}}\right)\right.\right.\\ &\left.\left.-\frac{\lambda(z-z_1)}{D(\sigma_{0,z_0},\sigma_{1,z_1})^2}\frac{\sigma_{0,z_1}}{\sigma_{0,0}}\left(\frac{(x-x_1)}{\lambda(z-z_1)}-\mathbf{i}\,\frac{(x_1-x_0)}{4\pi\sigma_{0,0}\sigma_{0,z_0}}\right)^2\right]\right\}.\end{aligned} \tag{37}$$

Here a factor A_∞ replaces $\sqrt{m/(2\pi\mathbf{i}\hbar T)}$. Since at $T\to\infty$ the quadratic root tends to zero, then $A_{\infty\,t}$ ends to zero as well. We will ignore this fact, and suppose let A_∞ be some innitesimal constant.

The wave function (37) describes interference eects emergent both behind the second grating $G1$ and between the gratings G_0 and G_1. In order to get the wave pattern between these gratings it is sucient to set $z_1 = z$ and $x_1 = x$. In this case, σ_1, z_1 becomes $\sigma_{1,0}$ and D (σ_0, z_0, σ_1, z_1) reduces to (σ_0, z_0 / $\sigma_{0,0}$)$^{1/2}$. Computations of the parameters ($\sigma_{0,0}$ and ($\sigma_{0,z0}$ are given in Eq. (17) on page 5. All terms in (37) containing dierences ($x - x_1$) and ($z - z_1$) disappear. To put it directly, all terms in (36) and (37) colored in blue are removed.

Citation: Valeriy I. Sbitnev (2021) Matter Waves in the Talbot-Lau Interferometry. Journal of Physics & Optics Sciences. SRC/JPSOS/163.
DOI: doi.org/10.47363/JPSOS/2021(3)150

Now, we can write out the wave function from N-slits grating as the result of the superposition of these truncated functions according to Eq. (25):

$$|\psi(x,z)\rangle = \frac{1}{N\sqrt{1+\mathrm{i}\dfrac{z\lambda_{\mathrm{dB}}}{2\pi b^2}}} \sum_{n=0}^{N-1} \exp\left\{ -\frac{\left(x-\left(n-\dfrac{N-1}{2}\right)d\right)^2}{2b^2\left(1+\mathrm{i}\dfrac{z\lambda_{\mathrm{dB}}}{2\pi b^2}\right)} \right\}. \tag{38}$$

Here the slit width is $b = b_0$, Eq. (14), λ_{dB} is de Broglie wavelength of the particle passing through the slit grating, and d is the slit spacing. Calculations of the interference patter gives perfect results [37]. Fig. 10 shows the density distribution $p(x, z) = \langle \psi(x, z) | \psi(x, z) \rangle$ in the very near zone of the N-slits grating for $N = 64$.

Let us now look at interference patterns emergent behind two gratings at illumination by matter waves with dierent wavelengths. Figs. 11(a) to 11(c) show interference patterns for incident particles having dierent de Broglie wavelengths:

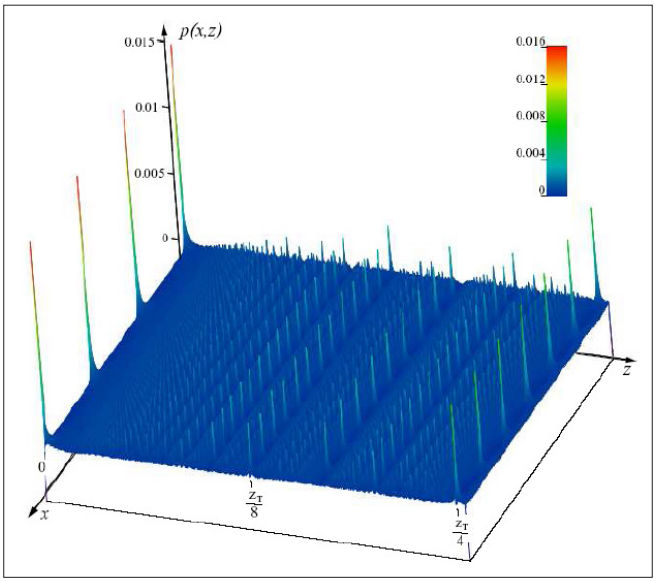

Figure 10: Density distribution pattern $p(x, z) = \langle \psi(x, z) | \psi(x, z) \rangle$ shown from central slits in very near zone. At a general amount of slits N = 64 a fractal structure is clearly visible. The wavelength is $\lambda_{\mathrm{dB}} = 5$ pm and the slit spacing $d = 40\,\lambda_{\mathrm{dB}} = 200$ pm

$\lambda_{\mathrm{dB}} = 3$ pm, $\lambda_{\mathrm{dB}} = 5$ pm, and $\lambda_{\mathrm{dB}} = 7$ pm. Velocities of the fullerene molecules at given wave-lengths are $vc_{60} \approx 110$ m/s, and vc_{60} 79 m/s respectively.

The grating G1 is situated at half of the Talbot length. Given $\lambda_{\mathrm{dB}} = 5$ pm and $d = 500$ nm the Talbot length is $z_T = 2d^2 / \lambda_{\mathrm{dB}} = 0.1$ m. Depending on the de Broglie wavelength chosen the interference pattern, emergent between the gratings discloses dierent scaling. Because of it, dierent interference patterns behind the second grating are formed. Most intensive the interference pattern arises at the de Broglie wavelength equal to 5 pm since the position of the grating G_1 has been tuned on the rst self-image of G_0 arising at the same wavelength.

One can observe a resonance eect at crossing the rst self-image of G_0 by the grating G_1. It can be achieved by changing the wavelength λ_{dB} at crossing the resonance condition $\lambda^{\mathrm{res}}_{\mathrm{dB}} = 2d / z_r$. In the case under consideration $\lambda^{\mathrm{res}}_{\mathrm{dB}} = 5$pm. Observe, that a maximal emittance from the grating G_1 is at $\lambda_{\mathrm{dB}} = \lambda^{\mathrm{res}}_{\mathrm{dB}}$, when it is positioned exactly on the rst self-image of G_0. There can be also high harmonics at $n\,\lambda_{\mathrm{dB}} = \lambda^{\mathrm{res}}_{\mathrm{dB}}$ (here n is integer), when G_1 is positioned on the high order images of G_0. In these cases, the emittance from G_1 quickly drops o with increasing n. The emittance to be expressed by a parameter (33) is shown in Fig. 12. Instead of representing via dependence of the de Broglie wavelength, here we show the dependence via the fullerene velocity $vc_{60} \approx h\,(mc_{60}\lambda_{\mathrm{dB}})$. Here h is the Planck constant. Evaluations say that for velocities 100 – 250 m/s one needs to support ultralow temperatures ranging from about $3 \cdot 10^{-3}$ to $3 \cdot 10^{-4}$ K.

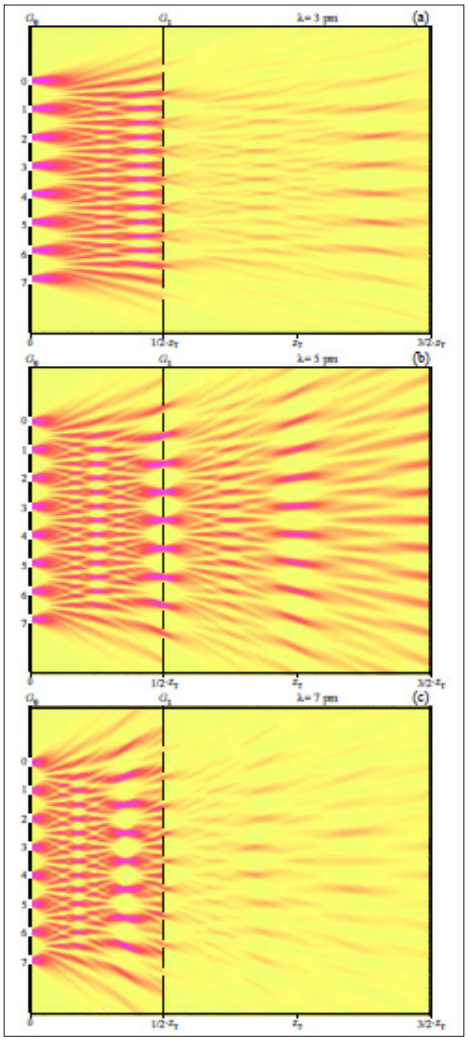

Figure 11: Density distribution pattern p(x,z) at dierent de Broglie wavelengths: (a) $\lambda_{\mathrm{dB}} = 3$pm, $vc_{60} \approx 184$ m/s; (b) $\lambda_{\mathrm{dB}} = 5$pm, $vc_{60} \approx 110$ m/s; (b) $\lambda_{\mathrm{dB}} = 7$ pm, $vc_{60} \approx 79$ m/s; $N_0 = 8$, $N_1 = 9$ and Talbot length $z_T = 0.1$ m.

Let us suppose that the remote source emits particles with dierent de Broglie wavelengths.

Citation: Valeriy I. Sbitnev (2021) Matter Waves in the Talbot-Lau Interferometry. Journal of Physics & Optics Sciences. SRC/JPSOS/163.
DOI: doi.org/10.47363/JPSOS/2021(3)150

Distribution over all wavelengths submits to the Gaussian with average λ_{dB} = 5 pm and dispersion constant σ_g = 2.25 pm. An averaged interference pattern for the wavelengths ranged from 3 pm to 8 pm with increment $\delta\lambda_{dB}$ = 0.25

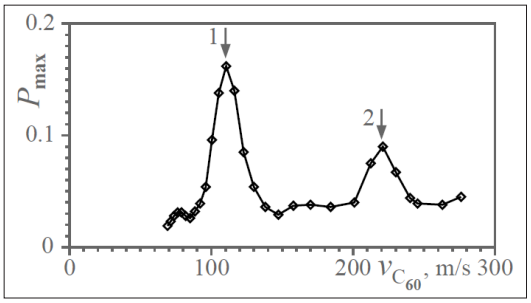

Figure 12: Emittance P_{max} in the cross-section $z = z_T$ vs velocity of the fullerene molecules. Arrows 1 and 2 point out the first and the second resonance harmonics.

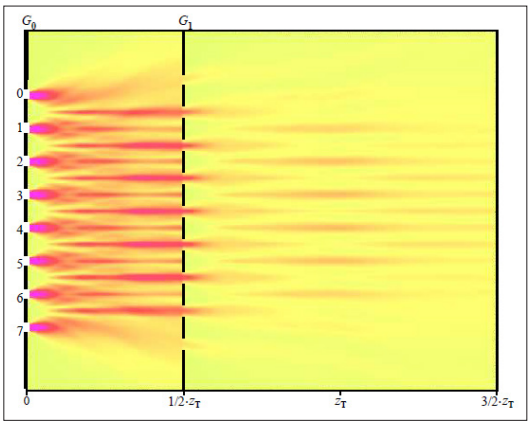

Figure 13: Density distribution pattern $p(x,z)$ at N_0 = 8, N_1 = 9 from a matter wave containing particles with dierent wavelengths from λ_{dB} = 2 pm to λ_{dB} = 8 pm

pm, and under the assumption that the sources are noncoherent, is shown in Fig. 13. One can see, that ne-structured details in the interference pattern disappear. They are simply washed out. Nairz, Arndt, and Zeilinger [8] has written for that occasion: "because the detector records the sum of the correspondingly stretched or com pressed diraction pictures, the interference pattern would be washed out. And in contrast to the spatial contribution, there is no gain in longitudinal (spectral) coherence during free flight." Fig. 13 conrms aforesaid thought. Interference patterns disclose equivalent image blur irrespective of choosing of the dispersion constant σ_g.

GRATINGS WITH MORE HARD-EDGED SLITS

Let us compute the path integral (4) for a case with more hardedged slits. With that aim, we should ll the slits uniformly by a number of the Gaussian functions (5) with more sharp bell curves. The step function, that simulates a single slit, can be approximated by the following a set of the Gaussian functions

$$G(\xi, b, \eta, K) = \frac{1}{\eta}\sqrt{\frac{2}{\pi}}\sum_{k=1}^{K}\exp\left\{-\frac{(K\xi - b(K-(2k-1)))^2}{2(b\eta)^2}\right\}. \quad (39)$$

Here parameter b is a half-width of the slit, real $\eta > 0$ is a tuning parameter, and K can take integer values. At $K \to \infty$ this function tends to an innite collection of the Kronecker deltas, that ll everywhere densely the step function.

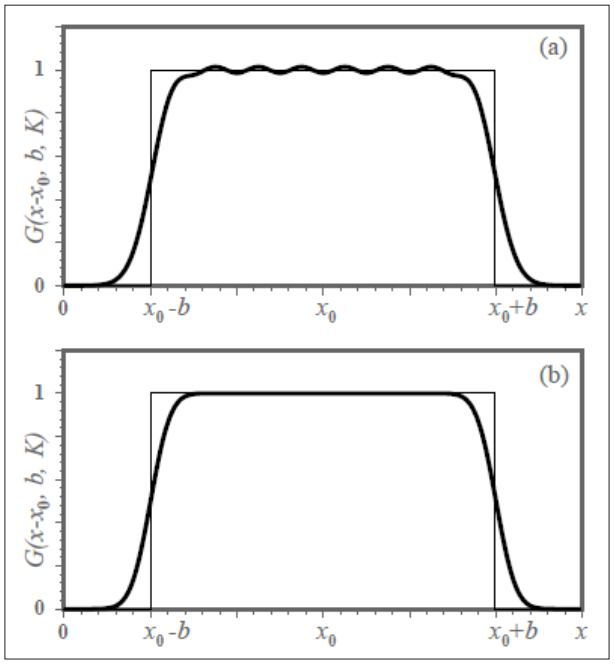

Figure 14: Approximation of the step function by set of the Gaussian functions presented in (39) with (a) η = 1, K = 8; and (b) η = 1.5, K = 16.

Fig. 14 shows approximation of the step function by the set of the Gaussian functions (39) with (a) η =1, K = 8 and η = 1.5, K = 16.

The form-factor G (ξ_1) in Eq. (6) is replaced here by the function $G(\xi_1, b_1, \eta_1, K_1)$. Solution of the integral (6), containing the set of the Gaussian functions (39), satises the formula

$$\frac{1}{\eta_1}\sqrt{\frac{2}{\pi}}\sum_{k=1}^{K_1}\int_{-\infty}^{\infty} e^{\alpha_k\xi^2+\beta_k\xi+\gamma_k}\,d\xi = \frac{1}{\eta_1}\sqrt{\frac{2}{\pi}}\sum_{k=1}^{K_1}\sqrt{\frac{\pi}{-\alpha_k}}\,e^{-\beta_k^2/4\alpha_k+\gamma_k}. \quad (40)$$

Before calculating the parameters $\alpha_k, \beta_k, \gamma_k$, we need to expand the square in Eq. (39): $(K\xi - b(K-(2k-1)))^2 = K^2\xi^2 - 2Kb(K-2k+1)\xi + b^2(K-2k+1)^2$. After that, we nd

1. the term at ξ_1^2:

$$\alpha_k = \frac{\mathbf{i}m}{2\hbar}\left(\frac{1}{\tau_1}+\frac{1}{\tau_0}+\mathbf{i}\,\frac{\hbar}{m\eta_1^2}\frac{K_1^2}{b_1^2}-\frac{1}{\tau_0^2(1/\tau_0+1/T+\mathbf{i}\hbar/mb_0^2)}\right); \tag{41}$$

2. the term at ξ_1:

$$\begin{aligned}\beta_k \;=\; -2\,\frac{\mathbf{i}m}{2\hbar}\Bigg(&\frac{(x_2-x_1)}{\tau_1}-\frac{(x_1-x_0)}{\tau_0}+\frac{(x_1-x_0)/\tau_0^2-(x_0-x_s)/\tau_0T}{(1/\tau_0+1/T+\mathbf{i}\hbar/m\,b_0^2)}\\ &+\;\mathbf{i}\,\frac{\hbar}{m\eta_1^2}\frac{K_1}{b_1}(K_1-(2k-1))\Bigg);\end{aligned} \tag{42}$$

3. the term free from ξ_1:
:

$$\begin{aligned}\gamma_k \;=\; \frac{\mathbf{i}m}{2\hbar}\Bigg(&\frac{(x_2-x_1)^2}{\tau_1}+\frac{(x_1-x_0)^2}{\tau_0}+\frac{(x_0-x_s)^2}{T}-\frac{((x_1-x_0)/\tau_0-(x_0-x_s)/T)^2}{(1/\tau_0+1/T+\mathbf{i}\hbar/mb_0^2)}\\ &+\;\mathbf{i}\,\frac{\hbar}{m\eta_1^2}(K_1-(2k-1))^2\Bigg).\end{aligned} \tag{43}$$

It is instructive to compare these parameters with those presented in Eqs. (8), (9), and (10). Dierences easily strike the eye. The amplitude factor (12) for our new task reads

$$A=\frac{1}{\eta_1}\sqrt{\frac{2}{\pi}}\cdot\sqrt{\frac{m}{\mathbf{i}\,2\pi\,\hbar T}}\cdot\frac{1}{D(b_0,b_1)}. \tag{44}$$

A minor dierence of the amplitude factors (12) and (44) is due to the additional factor $(2/\pi)^{1/2}/\eta_1 \approx 1.5$ and $K_1 = 1$ the amplitude factor (44) will be twice as little of the factor (12). The denominator $D(b_0, b_1)$ here has the following view

$$D(b_0,b_1)=\sqrt{\left(1+\frac{\tau_1}{\tau_0}\right)\left(1+\frac{\mathbf{i}K_1^2\hbar\tau_1}{m\,\eta_1^2\,b_1^2(1+\tau_1/\tau_0)}\right)\left(1+\frac{\tau_0}{T}\right)\left(1+\frac{\mathbf{i}\hbar\tau_0}{m\,b_0^2(1+\tau_0/T)}\right)-\frac{\tau_1}{\tau_0}}. \tag{45}$$

In turn, the therm $\gamma_k-\beta_k^2/4\alpha_k$ reads

$$\begin{aligned}\gamma_k-\beta_k^2/4\alpha_k = \frac{\mathbf{i}m}{2\hbar}\Bigg[&\left(\frac{(x_2-x_1)^2}{\tau_1}+\frac{(x_1-x_0)^2}{\tau_0}+\frac{(x_0-x_s)^2}{T}-\frac{((x_1-x_0)/\tau_0-(x_0-x_s)/T)^2}{((\tau_0+T)/T\tau_0+\mathbf{i}\hbar/m\,b_0^2)}\right.\\ &\left.+\,\mathbf{i}\,\frac{\hbar}{m\,\eta_1^2}(K_1-(2k-1))^2\right)\\ -\frac{\left(\frac{(x_2-x_1)}{\tau_1}-\frac{(x_1-x_0)}{\tau_0}+\frac{(x_1-x_0)/\tau_0-(x_0-x_s)/T}{\tau_0((\tau_0+T)/T\tau_0+\mathbf{i}\hbar/m\,b_0^2)}+\mathbf{i}\,\frac{\hbar}{m\,\eta_1^2}\frac{K_1}{b_1}(K_1-(2k-1))\right)^2}{\left(\frac{\tau_0+T}{T\tau_0}+\frac{\mathbf{i}\hbar}{m\,b_0^2}\right)^{-1}\frac{1}{\tau_0\tau_1 D(b_0,b_1)}}&\Bigg]\end{aligned} \tag{46}$$

Series of Replacements

In order to execute series of the replacements as in Subsec. IIA it is proposed to introduce the following scaling change for the half-width b_1

$$\frac{\eta_1 b_1}{K_1} \to b_1'. \tag{47}$$

From here we will have in mind that the parameters $\sigma_{1,0}$, $\sigma_{1,T1}$, $\Sigma_{1,z1}$ dened in Eqs. (14), (15), 18) can contain the very terms K_1 and η_1. After that, the parameters $\Sigma_{0,z0}$ and $\Sigma_{1,z1}$ in this task is rewritten as follows

$$\Sigma_{0,z_0} = \frac{z_1 - z_s}{z_0 - z_s} + \mathbf{i}\frac{\lambda(z_1 - z_0)}{4\pi\sigma_{0,0}^2}, \tag{48}$$

$$\Sigma_{1,z_1} = \frac{z_2 - z_0}{z_1 - z_0} + \mathbf{i}\frac{\lambda(z_2 - z_1)}{4\pi\sigma_{1,0}^2}\frac{K_1^2}{\eta_1^2}. \tag{49}$$

Here $\sigma_{0,0}$ and $\sigma_{1,0}$ have the original forms presented in (14).

The phase term $\gamma_k - \beta_k^2/4\alpha_k$ that has a rather complicated form (46), reads

$$\gamma_k - \beta_k^2/4\alpha_k = \mathbf{i}\pi\left[\left(\frac{(x_2-x_1)^2}{\lambda(z_2-z_1)} + \frac{(x_1-x_0)^2}{\lambda(z_1-z_0)}\left(1 - \frac{\Xi_0^2}{\Sigma_{0,z_0}}\right) + \frac{(x_0-x_s)^2}{\lambda(z_0-z_s)} + \mathbf{i}\frac{(K_1-(2k-1))^2}{2\pi\,\eta_1^2}\right)\right.$$
$$\left. - \frac{\lambda(z_2-z_1)\Sigma_{0,z_0}}{D(\Sigma_{0,z_0},\Sigma_{1,z_1})^2}\left(\frac{(x_2-x_1)}{\lambda(z_2-z_1)} - \frac{(x_1-x_0)}{\lambda(z_1-z_0)}\left(1-\frac{\Xi_0}{\Sigma_{0,z_0}}\right) + \mathbf{i}\frac{K_1(K_1-(2k-1))}{2\pi\,\eta_1^2\,b_1}\right)^2\right], \tag{50}$$

Here $D(\Sigma_{0,z0}, \Sigma_{0,z1})$ is represented in (22), but with 1;z1 is loaded from (49).

Now we can write the wave functions describing the appearance of a particle both between the gratings and behind the second grating.

Matter Waves behind the Gratings G_0 and G_1

A particle evolving from a single slit in G_0 forward to G_1 is described by the wave function (24):

$$\psi(x,z,x_0,x_s) = \sqrt{\frac{m}{\mathbf{i}2\pi\hbar T\Sigma_{0,z_0}}}\cdot\exp\left\{\mathbf{i}\pi\left[\frac{(x-x_0)^2}{\lambda(z-z_0)}\left(1-\frac{\Xi_0^2}{\Sigma_{0,z_0}}\right) + \frac{(x_0-x_s)^2}{\lambda(z_0-z_s)}\right]\right\}. \tag{51}$$

Observe that equivalence of the wave functions (51) and 24) is due to the fact that we use the same grating G_0 in both cases. But behind the grating G_1, having more hard-edged slits, movement of the particle from a single slit in in this grating is described by a wave function

$$\psi(x,z,x_1,x_0,x_s,K_1) = \frac{1}{\eta_1}\sqrt{\frac{2}{\pi}}\cdot\frac{\sqrt{\frac{m}{\mathbf{i}2\pi\hbar T}}}{D(\Sigma_{0,z_0},\Sigma_{1,z_1})}\sum_{k=1}^{K_1}$$
$$\exp\left\{\left[\left(\frac{(x-x_1)^2}{\lambda(z-z_1)} + \frac{(x_1-x_0)^2}{\lambda(z_1-z_0)}\left(1-\frac{\Xi_0^2}{\Sigma_{0,z_0}}\right) + \frac{(x_0-x_s)^2}{\lambda(z_0-z_s)} + \mathbf{i}\frac{(K_1-(2k-1))^2}{2\pi\,\eta_1^2}\right)\right.\right.$$
$$\left.\left. - \frac{\lambda(z-z_1)\Sigma_{0,z_0}}{D(\Sigma_{0,z_0},\Sigma_{1,z_1})^2}\left(\frac{(x-x_1)}{\lambda(z-z_1)} - \frac{(x_1-x_0)}{\lambda(z_1-z_0)}\left(1-\frac{\Xi_0}{\Sigma_{0,z_0}}\right) + \mathbf{i}\frac{K_1(K_1-(2k-1))}{2\pi\,\eta_1^2\,b_1}\right)^2\right]\right\}. \tag{52}$$

One can see, that with $K_1 = 1$ the wave function (52), accurate to the factor $(2/\pi)^{1/2}/\eta_1$) simply the function (23).

Interference patterns arise as superpositions of the above wave functions radiated from all slits of the grating G_0 and from all slits of the grating G_1. These wave functions of the matter waves emitted from all slits of the gratings G_0 and G_1 have been written out in Eqs. (25) and (26).

Note only, that the wave function $|\Psi\rangle$ contains extra parameters, integer K_1 and real η_1.

Citation: Valeriy I. Sbitnev (2021) Matter Waves in the Talbot-Lau Interferometry. Journal of Physics & Optics Sciences. SRC/JPSOS/163.
DOI: doi.org/10.47363/JPSOS/2021(3)150

Figs. 15(a), 15(b), and 15(c) show interference patterns emergent behind gratings containing only $N_0 = 4$ and $N_1 = 5$ slits. Slits of the grating G_1 are simulated by the set of the Gaussian functions (39) with the parameter η_1 equal to 1:5 and for dierent K_1 : (a) $K_1 = 1$; (b) $K_1 = 4$; and (c) $K_1 = 16$. More rapid divergence of the rays near the slits is seen to arise in the case of large K_1. These divergent rays induce nely ruled interference fringes arising before the rst Talbot length z_T, see Fig. 15 (c).

Observe, that behind double the Talbot length, $2z_T$ the interference fringes become equivalent independently of choosing K_1. Qualitative dierence of intensities seen in Fig. 15 (a), on the one hand, and in Figs. 15(b)-15(c), on the other hand, is due to presence of the factor $(2/\pi)^{1/2} / \eta_1 \approx 0.5$. This factor provides a good coincidence of a top plateau of the function (39) with that of the step function for $K_1 > 1$. Whereas in the case of $K_1 = 1$, the height of the Gaussian function becomes twice as little. In particular, the intensity in Fig. 15(a) is also twice as little as that in Fig. 4(a) for the same reason.

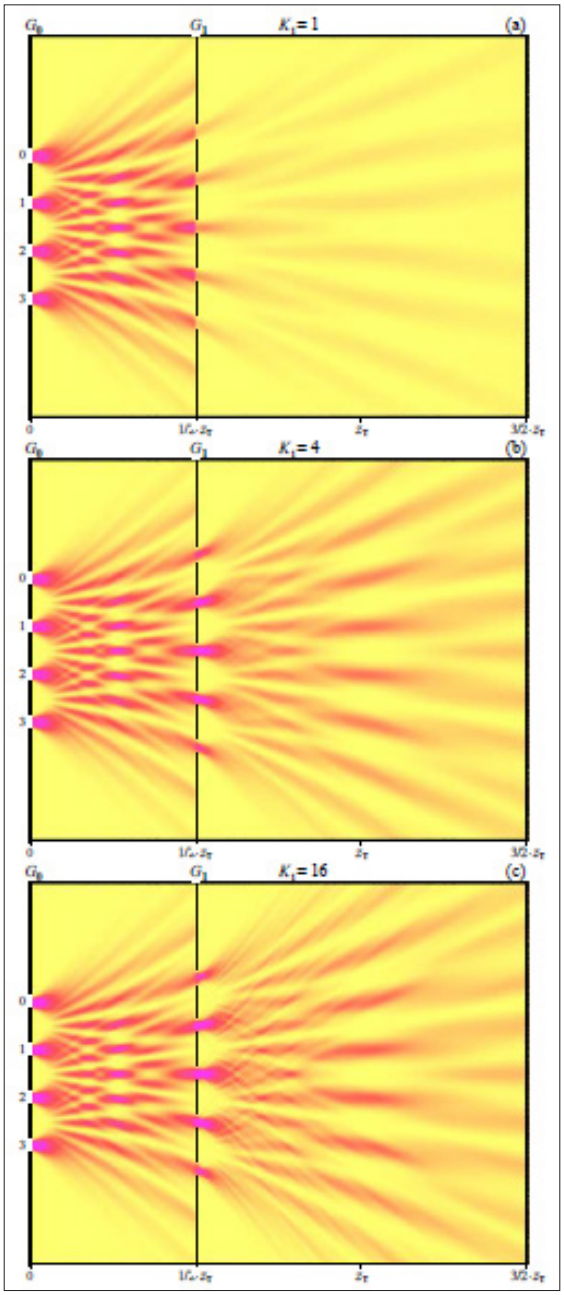

Figure 15: Density distribution pattern $p(x, z)$ in the near-eld region $z \in (0, 1.5\ z_T) = (0; 0{:}15)$ m, $N_0 = 4$, $N_0 = 5$, de

One can observe a surprising phenomenon nearby the slits of the grating G_1 as K_1 increases – the larger K_1 the better. The beam outgoing from a slit, rst, goes through focusing. After it passes the smallest diameter (it overcomes so-called the beam waist [32]) the beam begins to diverge. A detail pattern of this phenomenon in the vicinity of the central slit of G_1, see Fig. 15(c), is demonstrated in Fig. 16(a). The outgoing intensity pattern shown in a range from 0:5 z_T to 0.6 z_{Ti} is seen to have a complex organization. A tongue-like "jet" outgoing from the slit, rst, undergoes squeezing. Dark patches are places where the intensity reaches maximal values. The most maximal value is reached where the "jet" goes through the beam waist. Well- organized small dark patches seen in the gure precede the darkest central patch. These small

Broglie wavelength $\lambda_{dB} = 5$ pm, Talbot length $z_T = 0.1$ m. Distance from G_0 to the source is $z_s = -0.5$ m, $x_s = 0$ μm : (a) $K_1 = 1$; (b) $K_1 = 4$; (c) $K_1 = 16$. For all cases $\eta_1 = 1.5$.

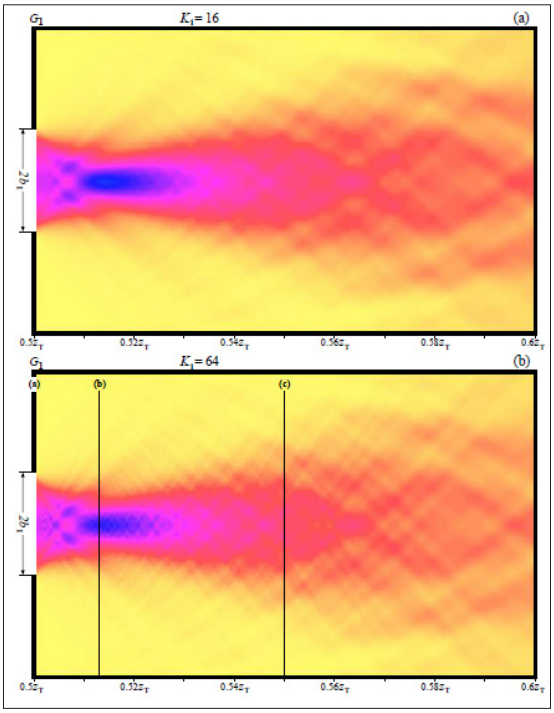

Figure 16: Cutting out radiation from the central slit of G_1 shown in Fig. 15(c): (a) reproduced for case of $K_1 = 16$; (b) reproduced for case of $K_1 = 64$. Blue patches near the slit are the most higher intensities of the radiation.

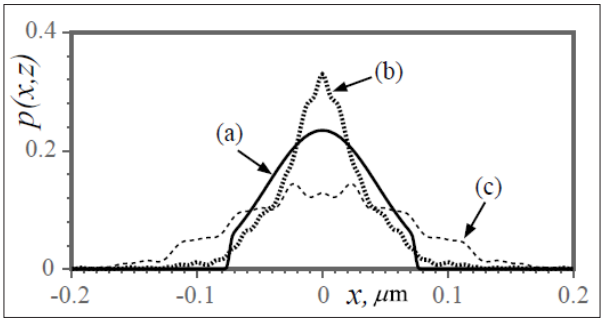

Figure 17: Proles of the probability density $p\ (x, z)$ within cross-sections (a) $z = 0.5\ z_T$ = (b) $z = 0.513\ z_T$; (c) $z = 0.55\ z_T$ of the interference pattern shown in Fig. 16.

Citation: Valeriy I. Sbitnev (2021) Matter Waves in the Talbot-Lau Interferometry. Journal of Physics & Optics Sciences. SRC/JPSOS/163.
DOI: doi.org/10.47363/JPSOS/2021(3)150

dark patches originate from the center of the slit. And as they approach towards the darkest central patch, weak divergent rays can be seen are radiated far aside. More detailed jet outgoing pattern simulated for $K_1 = 64$ is shown in Fig. 16(b).

Fig. 17 shows some proles of the probability density $p(x, z)$ taken from the interference pattern, that is obtained at given $K_1 = 64$ and $\eta_1 = 1.5$, Fig. 16(b). Integrals along the proles give almost equal values. Insignicant discrepancies are conditioned by the dissipation of the matter wave behind the integration interval.

The proles (a), (b), and (c) depicted in Fig. 17 are captured from cross-sections, that are marked by lines (a), (b), and (c) in Fig. 16(b). They are at $z = 0{:}5z_T$, $z = 0{:}513z_T$, and $z = 0{:}55z_T$, respectively. The prole (a) abuts on the slit screen. We can see in Fig. 17 that the prole (b) demonstrates against the background of the prole (a) a squeezing of the beam together with increasing its intensity along the center. Next, the beam begins to disperse as the distance from the slit increases, see, for example, the prole (c) in the same figure.

Emergence of the Focusing Spot

The emergence of the focusing spot with the increasing number of the Gaussian functions in (39), i.e., with increasing K_1 is an astonishing phenomenon at shaping slits with more hard edges. An eect of squeezing particle beam right after the slit can be understood at choosing of the slits that are approximated by the curve (39) with small K_1 and η_1. Let us study such an effect (a) with increasing K_1 at xed η_1; and (b) with increasing η_1 at xed K_1.

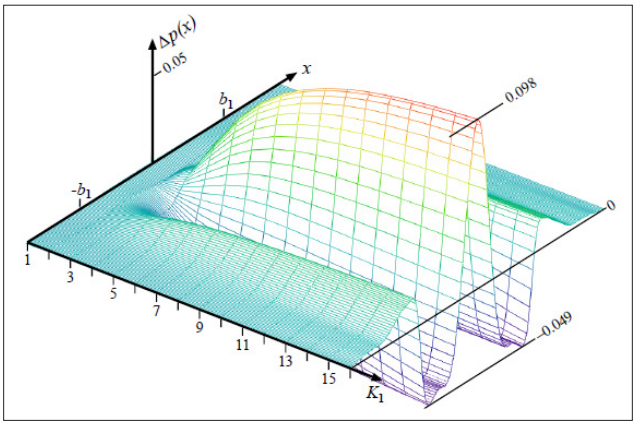

Figure 18: Dierence $\Delta p(x)$ of two proles of the probability density $p(x, z)$ given on the slit ($z_a = 0.5\ z_T$) and in the crosssection of the beam waist ($z_b = 0.513\ z_T$) as a function of K_1. The real parameter η_1 is equal to 1.5.

Let us consider, rst, the emergence of the focusing spot with increasing integer K_1 from 1 to 16 at fixed $\eta_1 = 1.5$. For this aim, we propose to evaluate a dierence of two proles of the probability density $p(x, z)$ given on the slit ($z_a = 0{:}5z_T$) and in the cross-section of the beam waist ($z_b = 0{:}513z_T$):

$$\Delta p(x) = p(x, z_b) - p(x, z_a). \qquad (53)$$

As seen in Fig. 17 this dierence can have a large positive hill in the center of the beam bounded by wells from both sides. All lies within a space of the slit. Fig. 18 shows a series of the differences $\Delta p(x)$ to be calculated for $K1$ ranging from 1 to 16 and at fixed $\eta_1 = 1{:}5$. One can see, given K_1 equal to 1 there is no $\Delta p(x)$ different from zero. As K_1 increases from 1 to 16 $\Delta p(x)$ grows quickly enough and at $K_1 = 16$ its peak reaches almost 0:1. It is the focusing spot bounded by the wells from both sides. The depth of the wells is about –0:05 and they lie between edges of the slit, between $-b_1$ and b_1. The dif-
ference (53) brings to light the focusing eect of outgoing from the slit the beam well enough.

Let us now consider shaping the focusing spot with increasing η_1 but at fixed K_1. For deniteness, we will choose integer $K_1 = 7$ and real η_1 ranging 0:2, 0:5, and 0:8, all are smaller than 1, see Fig. 19. Integrals of the approximating curves are equal to a square of the step function for all cases.

As seen in Fig. 19(a), the rst curve simulates seven slits situated within the interval $[-b;+b]$. Let $2b_1 \approx 150$ nm, then a period of such a nely ruled grating is about 20 nm. It corresponds to about 50 atoms situated between nely cut slits. The Talbot length, $z_T = 0.1$ m, earlier computed represents a very large length as against a Talbot length, $z_T \sim 10^{-4}$ m, for the nely ruled grating having short intervals between the nely cut slits. We may observe in that connection series of principal diraction maxima from this finely cut grating. These maxima are partitioned by $(K_1 - 2) = 5$ subsidiary maxima [29]. All these rays are divergent in the far-eld region of the finely ruled grating which, in turn, is situated within the near-eld region of the grating G_1.

The above-described picture is shown in Fig. 20(a). One can see, that a central principal ray, diverging forward from miniature Talbotclusters packed by a triangle-like manner, has a narrow width before it will begin to diverge fur ther. The width is positioned within $z \approx 0.512\ z_T$ to $z \approx 0.524\ z_T$. Positions of these two points in

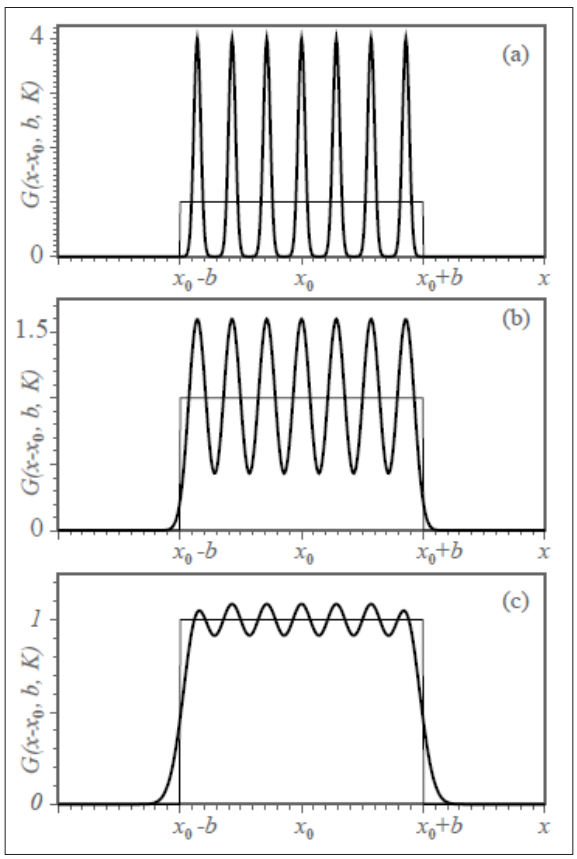

Figure 19: Approximation of the step function by set of the Gaussian functions presented in (39) with integer $K = 7$ and real (a) $\eta = 0{:}2$; (b) $\eta = 0{:}5$; (c) $\eta = 0{:}8$.

Fig. 20 are marked by vertical lines.

Let us look on the second and the third curves in Figs. 19(b) and 19(c), that have been simulated at c = 0:5 and η_1 = 0:8, respectively. We see, rst, because of the emergence of a pedestal under the function (39) at increasing the parameter η, the intensity of radiation from the slits grows up considerably. With increasing the parameter η the function has a trend to approximate to the step function. Observe that the intensity of the radiation from the slit becomes the larger the more precise the function (39) approximates the step function. At increasing the parameter η the triangle-like pattern near the slit is seen to dissolve in the main ray. Together with that, the focusing spot is formed after the point $z \approx 0.512\ z_T$ As the approximating function approximates to the step function, the focusing spot of the slit's beam becomes apparent within the interval from $0.512\ z_T$ to $0.524\ z_T$, see Figs. 20(b) and 20(c). This is an interval where rays formative the central principal maximum undergo squeezing in front of subsequent divergence [29]. Fig. 20(d) shows a formed beam right away after the slit in case of the parameter $\eta > 1$.

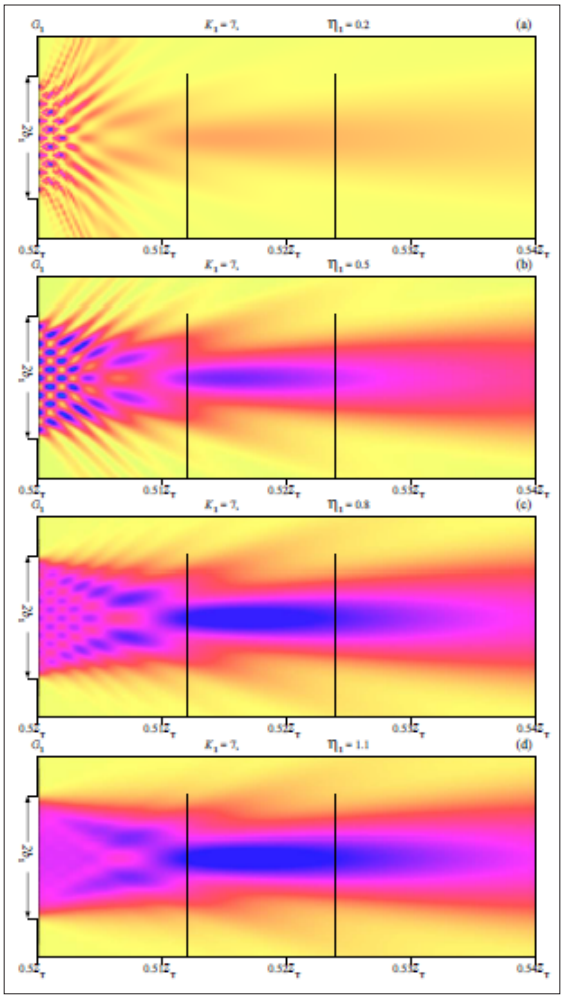

Figure 20: Density distribution pattern p (x, z) right after the grating G_1: z ∈ ($0.5z_T$, $0.54z_T$) and x ∈ (–125, 125) nm: (a) η = 0:2; (b) η = 0:5; (c) η = 0:8; (d) η = 1:1. K_1 = 7 and N_0 = 2, N_1 = 1. De Broglie wavelength λ_{dB} = 5 pm, width of the slit $2b_1$ = 150 nm, and Talbot length z_T = 0.1 m.

Conclusion

Developed by Richard Feynman the path integral method [21] represents by itself a very powerful instrument for calculation dierent situa tions in the interference problems. By utilizing this method, we have computed the interference pattern from two gratings, placed in consecutive order along a particle beam. A wave function describing the interference is found by summing all possible trajectories of the particles passing through slits in the rst grating and then in the second grating. This powerful method permits a description of the interference eects of the matter waves in detail.

It is instructive to attract attention to the manifestation of wave-particle duality nature at describing the wave processes by this method. At rst, we begin to consider particle paths going from a source to a detector through all possible intermediate points. Ensemble of all possible paths describes the eect of propagation of a matter-wave. Wavefronts are represented by equal phase surfaces that secant the trajectory bundles. Observe, that these waves are those that underlie the Huygens-Fresnel principle [38].

The wave function found by the path integral method gives a clear picture of the interference both between the gratings and behind the second grating. The most impressive observation of the interference eect is the emergence of the Talbot- like carpets. These interference patterns demon- strate a fractal organization when the amount of the slits and the slit spacing increase to infinity, But at an illumination of the gratings by incoherent matter waves, the carpets and their fractal peculiarities are smeared out. The emergence of pedestals, supporting the interference fringes, and decreasing the visibility are conditioned by breaking the coherence of the beam that results in the smearing of the interference pattern. It conrms results obtained at the experimental observation of the interference fringes fullled on molecular beams [10, 12, 39].

The grating, prepared with more hard-edged slits, as was shown corrects particle ows in the vicinity of the slits the more powerfully than the grating with the fuzzy-edged slits. An astonishing eect of the more hard-edged slits is that they shape focusing spots of the particle beam just after the slits. Next, they disperse along the beam with producing ripples. The situation is the same as rays initially converging within a focus and diverging after. The focusing spot looks like a tongue-like jet passing through the beam waist. In particular, Nye [40] has shown that an electromagnetic monochromatic plane wave, incident on a perfectly conducting screen of vanishingly small thickness that contains an innitely long slit, reproduces behind this slit an analogous tongue-like EM jet. Increasing EM amplitude right after the slit is shown in this case as well. One may suppose, that the phenomenon of focusing by the slits having more hard edges is typical for many wave processes.

References

1. Cronin AD, Schmiedmayer J, Pritchard DE (2009) Optics and interferometry with atoms and molecules. Rev. Mod. Phys 81: 1051-1129.
2. Nowak S, Kurtsiefer Ch, Pfau T, David C (1997) High-order Talbot fringes for atomic matter waves. Optics Letters 22: 1430-1432.
3. Hackerm¨uller L, Hornberger K, Brezger B, Zeilinger A, Arndt M (2004) Decoherence of matter waves by thermal emission of radiation. Nature 427: 711-714.
4. Brezger B, Arndt M, and Zeilinger A (2003) Concepts for near-field interferometers with large molecules. J. Opt. B: Quantum Semiclass. Opt 5: 82-89.
5. Brezger B, Hackerm¨uller L, Uttenthaler S, Petschinka J, Arndt M, Zeilinger A (2002) Matter-wave interferometer for large molecules. Phys. Rev. Lett 88: 100404.
6. Hackerm¨uller L, Hornberger K, Brezger B, Zeilinger A, Arndt M (2003) Decoherence in a Talbot Lau interferometer: the influence of molecular scattering. Appl. Phys. B 77: 781-787.

7. Arndt M, Hackerm¨uller L, and Reiger E (2005) Interferometry with large molecules: Exploration of coherence, decoherence and novel beam methods. Brazilian Journal of Physics 35: 216-223.
8. Nairz O, Arndt M, Zeilinger A (2003) Quantum interference experiments with large molecules. Am. J. Phys 71: 319-325.
9. Yanov I, Leszczynski J (2004) Computer simulation of fullerenes and fullerites. In Computional materials science 85-115-p.
10. Juffmann T, Truppe S, Geyer P, Major AG, Deachapunya S, et al. (2009) Wave and particle in molecular interference lithography. Phys. Rev. Lett 103: 263601.
11. Hornberger K, Sipe JE, Arndt M (2004) Theory of decoherence in a matter wave Talbot-Lau interferometer. Phys. Rew. A 70: 053608.
12. Hornberger K, Hackerm¨uller L, Arndt M (2005) Influence of molecular temperature on the coherence of fullerenes in a near-field interferometer. Phys. Rew. A 71: 023601.
13. Nimmrichter S, Hornberger K (2008) Theory of nearfield matter wave interference beyond the eikonal approximation. Phys. Rew. A 78: 023612.
14. Hornberger K, Gerlich S, Ulbricht H, Hackerm¨uller L, Nimmrichter S, et al. (2009) Theory and experimental verification of kapitzadirac-talbot-lau interferometry. New Journal of Physics 11: 043032.
15. Cowley JM, Moodie AF (1957a) Fourier images: I - The point source. Proc. Phys. Soc. B 70: 486.
16. Cowley JM, Moodie AF (1957b) Fourier images: II - The out-of-focus patterns. Proc. Phys. Soc. B 70: 497.
17. Cowley JM, Moodie AF (1957c) Fourier images: III - Finite sources. Proc. Phys. Soc. B 70: 505.
18. Cowley JM, Moodie AF (1960) Fourier images IV: The phase grating. Proc. Phys. Soc 76: 378.
19. Schu¨ocker D, Schr¨oder K (1998) Optics, resonators and beams. In D. Schu¨ocker, editor, Handbook of the EuroLaser Academy 51-84-p.
20. Feynman RP (1948) Space-time approach to non-relativistic quantum mechanics. Phys. Rev. Lett 20: 367-387.
21. Feynman RP, A Hibbs A (1965) Quantum Mechanics and Path Integrals. McGraw Hill, New York.
22. Jahns J, Lohmann AW (1979) The Lau effect (a diffraction experiment with incoherent illumination). OPTICS COMMUNICATIONS 28: 263-267.
23. McMorran BJ, Cronin AD (2009) An electron Talbot interferometer. New Journal of Physics 11: 033021.
24. Mandel L, Wolf E (1995) Optical Coherence and Quantum Optics. Cambridge University Press, Cambridge.
25. Gbur G, Wolf E (2001) The Rayleigh range of Gaussian Schell-model beams. Journal of Modern Optics 48: 1735-1741.
26. McMorran B, Cronin AD (2008a) Model for partial coherence and wavefront curvature in grating interferometers. Phys. Rev. A 78: 013601
27. McMorran B, Cronin AD (2008b) Gaussian Schell source as model for slit-collimated atomic and molecular beams. URL http://arxiv.org/abs/0804.1162.
28. Ashmead J (2010) Quantum time. URL http://arxiv. org/abs/1005.0789.
29. Sbitnev VI (2010) N-slit interference: Path integrals, Bohmian trajectories. URL http://arxiv.org/abs/ 1001.0661.
30. Sanz AS, Miret-Artˆes S (2007) A causal look into the quantum Talbot effect. J. Chem. Phys 126: 234106.
31. Sanz AS, Miret-Artˆes S (2008) A trajectory-based understanding of quantum interference. J. Phys. A: Math. Gen 41: 435303.
32. Cronin AD, McMorran B (2006) Electron interferometry with nanogratings. Phys. Rev. A 74: 061602(R).
33. Berry M (1996) Quantum fractals in boxes. J. Phys. A: Math. Gen 29: 6617-6629.
34. Berry M, Klein S (1996) Integer, fractional and fractal Talbot effects. Journal of Modern Optics 43: 2139-2164.
35. Berry M, Marzoli I, Schleich W (2001) Quantum carpets, carpets of light. Physics World 6: 39-44.
36. Case WB, Tomandl M, Deachapunya S, Arndt M (2009) Realization of optical carpets in the Talbot and Talbot-Lau configurations. OPTICS EXPRESS 17: 20966-20974.
37. Sbitnev VI (2021) Quaternion algebra on 4d superfluid quantum space-time:can dark matter be a manifestation of the superfluid ether? Univere 7: 1-40.
38. Lanczos C (1970) The variational principles of mechanics. Dover Publ., Inc., N. Y.
39. Gerlich S, Hackerm¨uller L, Hornberger K, Stibor A, Ulbricht H, et al. (2007) A kapitza-dirac-talbot-lau interferometer for highly polarizable molecules. Nature Physics 3: 711-715.
40. Nye JF (2002) Numerical solution for diffraction of an electromagnetic wave by slits in a perfectly conducting screen. Proc. R. Soc. Lond. A 458: 401-427.